Massachusetts Institute of Technology
Artificial Intelligence Laboratory

A.I. Memo No. 910 July 1986

On Dynamic Models of Robot Force Control

Steven D. Eppinger
Warren P. Seering

Abstract

For precise robot control, endpoint compliance strategies utilize feedback from a force sensor located near the tool/workpiece interface. Such endpoint force control systems have been observed in the laboratory to be limited to unsatisfactory closed-loop performance. This paper discusses the particular dynamic properties of robot systems which can lead to instability and limit performance. A series of lumped-parameter models is developed in an effort to predict the closed-loop dynamics of a force-controlled single-axis arm. The models include some effects of robot structural dynamics, sensor compliance, and workpiece dynamics. The qualitative analysis shows that the robot dynamics contribute to force-controlled instability. Recommendations are made for models to be used in control system design.

Acknowledgments

This report describes research done at the Artificial Intelligence Laboratory of the Massachusetts Institute of Technology. Support for the laboratory's artificial intelligence research is provided in part by the System Development Foundation and in part by the Advanced Research Projects Agency of the Department of Defense under Office of Naval Research contract N00014-85-K-0124. Support for this research project is also provided in part by the TRW Foundation.

This research was originally presented in April 1986 at the IEEE International Conference on Robotics and Automation in San Francisco, California [2].

Introduction

Certain robot tasks demand precise interaction between the manipulator and its environment. Among these are many of the operations required in the mechanical assembly process. Strategies for the execution of such tasks involve controlling the relationship between endpoint forces and displacements under the environmentally-imposed constraints. This endpoint *compliance* can be implemented in many different schemes. Whitney [9] provides an overview of these.

Endpoint force control strategies depend upon force signals measured by a wrist sensor. The sensor output is fed back to the controller to alter the system's performance. Many such closed-loop systems have been built using various force control algorithms, and many stability problems have been observed. A theoretical treatment of environmentally-imposed constraints is provided by Mason [5], who also suggests a control methodology to augment these "natural" constraints with an appropriate set of "artificial" constraints. Raibert and Craig [6] developed a hybrid control architecture capable of implementing Mason's theory. Salisbury [8] showed that an end effector's stiffness could be controlled in Cartesian coordinates using an appropriately-formed joint stiffness matrix.

Active force control systems that have been implemented to test these strategies have demonstrated dynamic stability problems. Historically, some instabilities have been caused by digital sampling, and Whitney [9] discusses these conditions. Researchers have also observed the effects of unmodeled (uncompensated) nonlinearities, such as friction or backlash [4]. Raibert and Craig [6] implemented their hybrid controller and found sustained oscillations present in the controlled system. Instabilities have been observed in the operation of both of the force-controlled robots currently in use at the MIT Artificial Intelligence Laboratory. These robots include a PUMA arm and the new MIT Precision Assembly Robot. Both arms display performance differences when the workpiece (environment) characteristics are changed.

Roberts [7] investigated the effect of wrist sensor stiffness on the closed-loop system dynamics; he also included drive stiffness (transmission compliance) in his dynamic model. Transmission compliance causes the joint actuators and wrist sensors to be *noncolocated*, a condition discussed in detail by Gevarter [3]. Cannon [1] has investigated the similar problem of the position control of a flexible arm with endpoint sensing. He has shown that a high-order compensator is able to stabilize the system, but with limited bandwidth and high sensitivity to parameter changes.

Researchers have named many suspected causes of the instabilities observed in force-controlled robot systems. Among these are: low digital sampling rate, filtering, workpiece dynamics, environment stiffness, actuator bandwidth, sensor dynamics, arm flexibility,

impact forces upon tool/workpiece contact, and drive train backlash or friction. This paper addresses the effects of arm, sensor, and workpiece dynamics. Using conventional modeling and analysis techniques, it is demonstrated that when the arm flexibility gives rise to a vibratory mode within the desired closed-loop bandwidth, instability can occur. In particular, a simple, one-axis force control algorithm exhibits stable behavior when the higher-order dynamics of the arm can be neglected, and it can be unstable if those effects are significant. This is believed to be the cause of the instabilities observed in the robots at the MIT AI Laboratory.

Unstable behavior often takes the form of a limit cycle where the robot is making and breaking contact with the workpiece[1]. The discontinuous nature of this response makes the system difficult to model using linear elements. However, for the purposes of controller design, we will neglect the discontinuity and study linear system models. Nonlinear simulations suggest that if the linearized system has sufficient damping, then neglecting the discontinuity is justified. However, if the linearized system has unstable or highly oscillatory closed-loop poles, then the discontinuity should be included in the model so that limit cycles can be predicted in simulation.

Rigid Body Robot Model

To begin with a simple case, let us consider the robot[2] to be a rigid body, with no vibrational modes. Let us also consider the workpiece to be rigid, having no dynamics. The sensor connects the two with some compliance, as shown in Figure 1.

We model the robot as a mass with a damper to ground. The mass m_r represents the effective moving mass of the arm. The viscous damper b_r is chosen to give the appropriate rigid body mode to the unattached robot. The sensor has stiffness k_s and damping b_s. The workpiece is shown as a "ground state". The robot actuator is represented by the input force F and the state variable x_r measures the position of the robot mass.

The open-loop dynamics of this simple system are described by the following transfer function:

$$\frac{X_r(s)}{F(s)} = \frac{1}{m_r s^2 + (b_r + b_s)s + k_s}$$

---

[1] In this paper, the terms *workpiece* and *environment* are used interchangeably. The workpiece is the component of the environment contacted by the end effector of the force-controlled robot system.

[2] Throughout the model development, the term *robot* refers to the arm itself. The term *robot system* refers to the total system, comprised of the robot, sensor, workpiece, and controller.

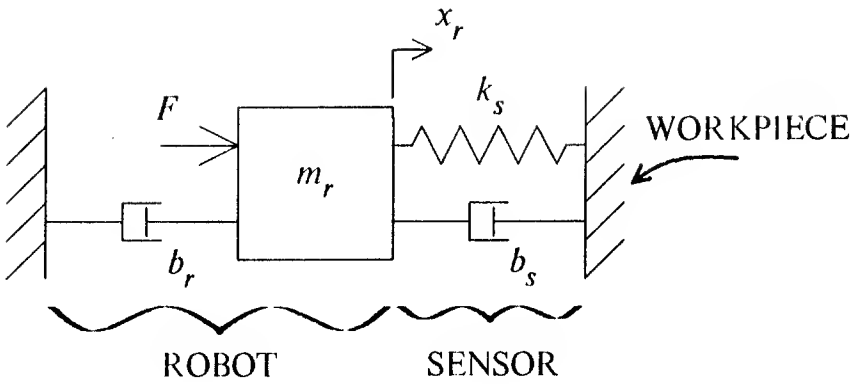

Figure 1: Rigid body robot model with compliant sensor and rigid workpiece.

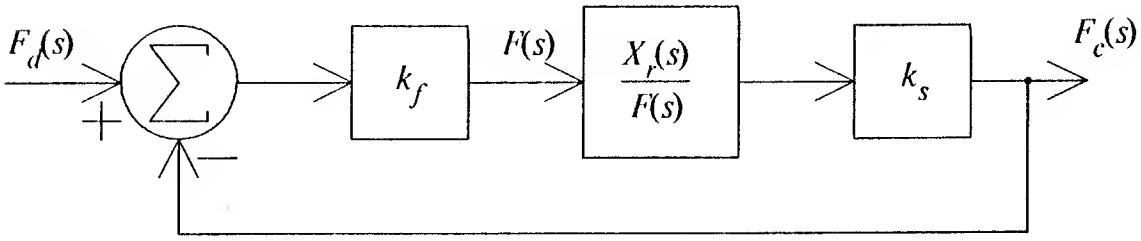

Figure 2: Block diagram for the controller of Figure 1.

Since this robot system is to be controlled to maintain a desired contact force, we must recognize that the closed-loop system output variable is the force across the sensor, the contact force F_c.

$$F_c = k_s x_r$$

We will now implement the simple proportional force control law:

$$F = k_f(F_d - F_c) \qquad (k_f \geq 0)$$

which states that the actuator force should be some nonnegative force feedback gain k_f times the difference between some desired contact force F_d and the actual contact force. This control law is embodied in the block diagram of Figure 2. The closed-loop transfer function then becomes

$$\frac{F_c(s)}{F_d(s)} = \frac{k_f k_s}{m_r s^2 + (b_r + b_s)s + k_s(1+k_f)}$$

The control loop modifies the characteristic equation only in the stiffness term. The force control for this simple case works like a position servo system. This could have been predicted from the model in Figure 1 by noting that the contact force depends solely upon the robot position x_r.

For completeness, let us look at the root locus plot for this system. Figure 3 shows the positions in the *s*-plane of the roots of the closed-loop characteristic equation as the force feedback gain k_f varies[3]. For $k_f=0$, the roots are at the open-loop poles. The loci show that as the gain is increased, the natural frequency increases, and the damping ratio decreases, but the system remains stable. In fact, k_f can be chosen to give the controlled system desirable response characteristics.

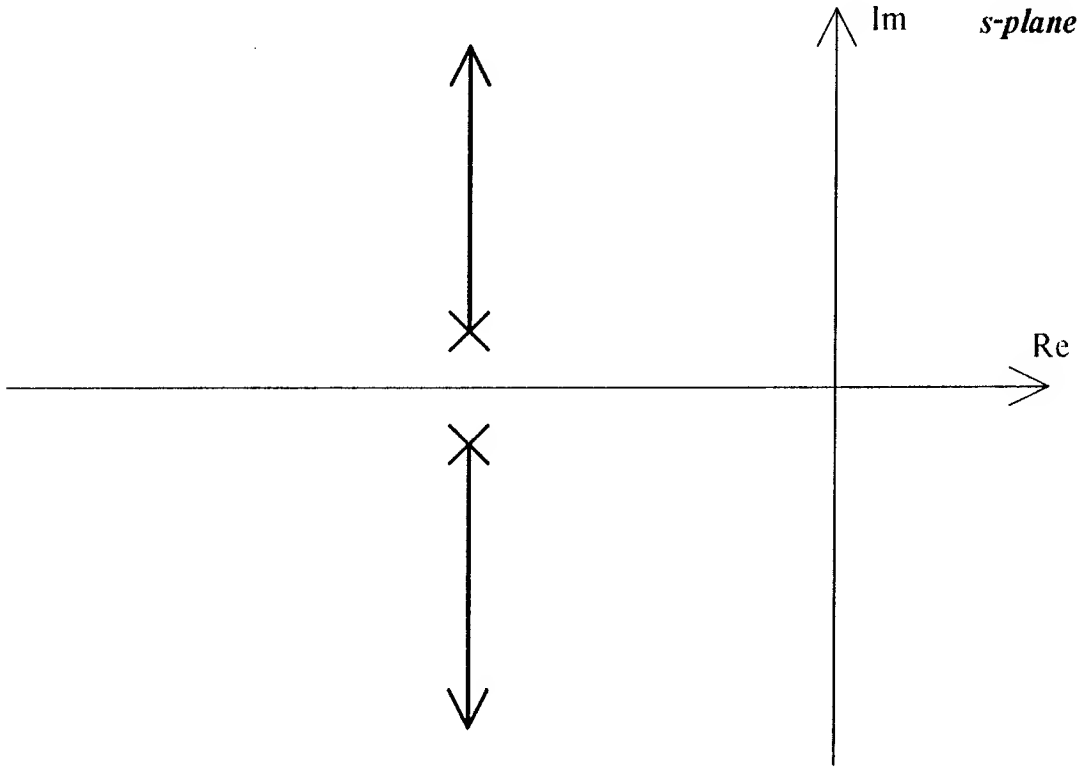

Figure 3: Root locus plot shape for the controller of Figure 1.

Include Workpiece Dynamics

The simple robot system of Figure 1 has been shown to be unconditionally stable (for $k_f \geq 0$). Force controlled systems, however, have been observed to exhibit variations in dynamic behavior depending upon the characteristics of the workpiece with which the robot is in contact. It is with this phenomenon in mind that the robot system model is augmented to include workpiece dynamics as shown in Figure 4.

---

[3]For this qualitative analysis, the model parameter values have been chosen only to plot root locus *shapes* representative of robot systems. They do not correspond to data taken from any specific robot. For this reason, the plots, do not contain numerical markings on the axes.

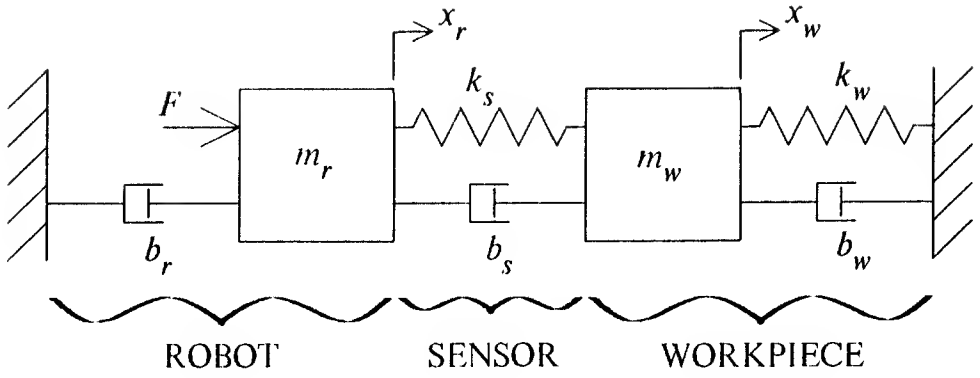

Figure 4: Rigid body robot model including workpiece dynamics.

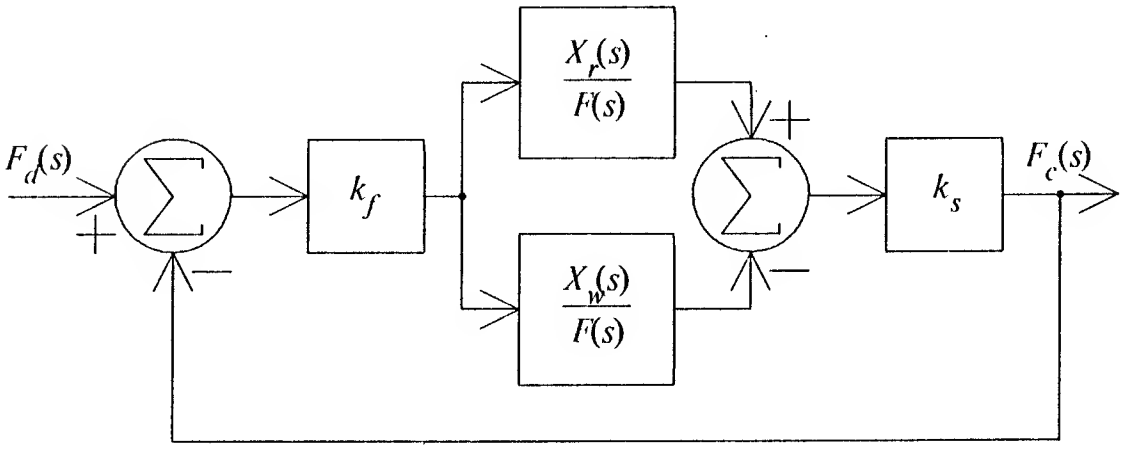

Figure 5: Block diagram for the controller of Figure 4.

This two-mass model includes the same robot and sensor models used above, with the workpiece now represented by a mass m_w. The workpiece is supported by a spring and damper to ground with parameters k_w and b_w, respectively. The new state variable x_w measures the position of the workpiece mass.

The open-loop transfer functions of this two degree-of-freedom system are:

$$\frac{X_r(s)}{F(s)} = \frac{m_w s^2 + (b_w + b_s)s + (k_w + k_s)}{\langle 4^{\text{th}}\text{-order characteristic polynomial}\rangle}$$

$$\frac{X_w(s)}{F(s)} = \frac{b_s s + k_s}{\langle 4^{\text{th}}\text{-order characteristic polynomial}\rangle}$$

where

$\langle 4^{\text{th}}$-order characteristic polynomial$\rangle$ =

$$[m_r s^2+(b_r+b_s)s+k_s][m_w s^2+(b_s+b_w)s+(k_s+k_w)] - [b_s s+k_s]^2$$

The output variable is again the contact force F_c, which is the force across the sensor, given by

$$F_c = k_s(x_r - x_w).$$

If we now implement the same simple force controller, the control law remains unchanged.

$$F = k_f(F_d - F_c) \qquad (k_f \geq 0)$$

The block diagram for this control system is shown in Figure 5. Note that the feedforward path includes the difference between the two open-loop transfer functions.

The root locus for this system is plotted in Figure 6 as the force feedback gain k_f is varied. There are four open-loop poles and two open-loop zeros. The plot then still has two asymptotes, at $\pm 90^{\circ}$. The shape of this root locus plot tells us that even for high values of gain, the system has stable roots. Therefore, while the characteristics of the workpiece affect the dynamics of the robot system, they do not cause unstable behavior.

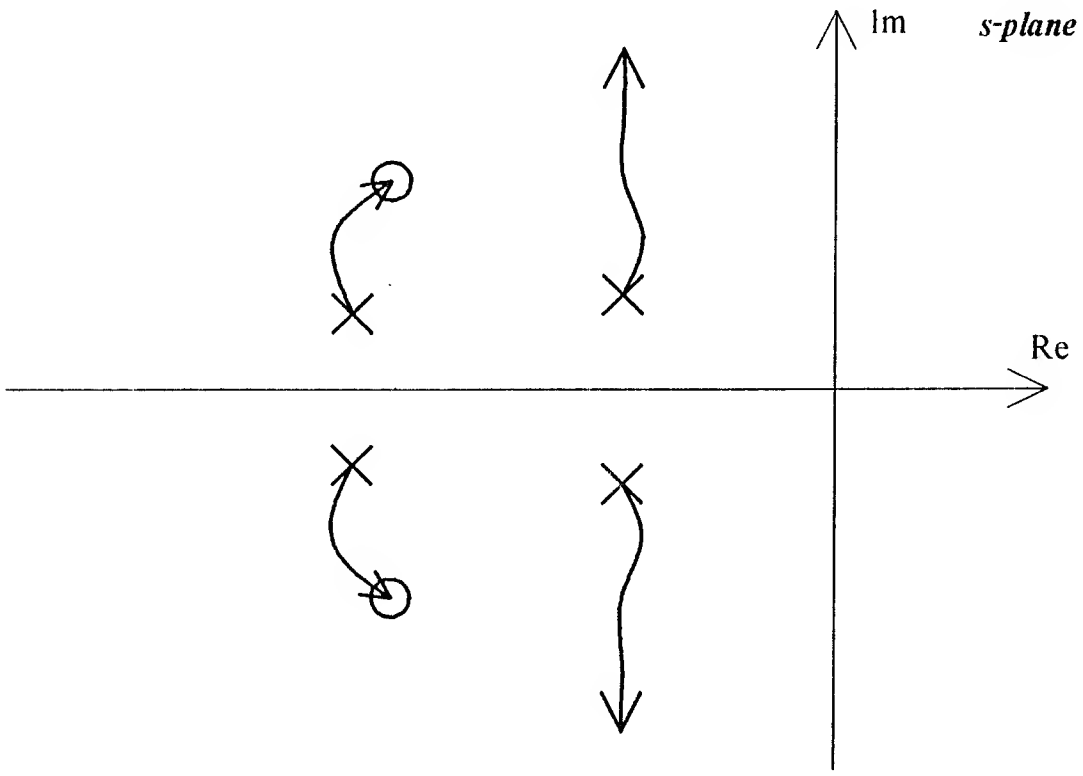

Figure 6: Root locus plot shape for the controller of Figure 4.

Include Robot Dynamics

Since the addition of the workpiece dynamics to the simple robot system model did not result in the observed instability, we will augment our system with a more complex robot model. If we wish to include both the rigid-body and first vibratory modes of the arm, then the robot alone must be represented by two masses.

Figure 7 shows the new system model. The total robot mass is now split between m_1 and m_2. The spring and damper with values k_2 and b_2 set the frequency and damping of the robot's first mode, while the damper to ground, b_1, primarily governs the rigid-body mode. The stiffness between the robot masses could be the drive train or transmission stiffness, or it could be the structural stiffness of a link. The masses m_1 and m_2 would then be chosen accordingly. The sensor and workpiece are modeled in the same manner as in Figure 4. The three state variables x_1, x_2, and x_w measure the positions of the masses m_1, m_2, and m_w.

This three-mass model has the following open-loop transfer functions:

$$\frac{X_1(s)}{F(s)} = \frac{\langle 4^{\text{th}}\text{-order numerator polynomial}\rangle}{\langle 6^{\text{th}}\text{-order characteristic polynomial}\rangle}$$

$$\frac{X_2(s)}{F(s)} = \frac{\langle 3^{\text{rd}}\text{-order numerator polynomial}\rangle}{\langle 6^{\text{th}}\text{-order characteristic polynomial}\rangle}$$

$$\frac{X_w(s)}{F(s)} = \frac{\langle 2^{\text{nd}}\text{-order numerator polynomial}\rangle}{\langle 6^{\text{th}}\text{-order characteristic polynomial}\rangle}$$

where

$\langle 4^{\text{th}}\text{-order numerator polynomial}\rangle =$

$$[m_2s^2+(b_2+b_s)s+(k_2+k_s)]\,[m_ws^2+(b_s+b_w)s+(k_s+k_w)] - [b_ss+k_s]^2$$

$\langle 3^{\text{rd}}\text{-order numerator polynomial}\rangle =$

$$[m_ws^2+(b_s+b_w)s+(k_s+k_w)][b_2s+k_2]$$

$\langle 2^{\text{nd}}\text{-order numerator polynomial}\rangle =$

$$[b_2s+k_2][b_ss+k_s]$$

$\langle 6^{\text{th}}\text{-order characteristic polynomial}\rangle =$

$$[m_1s^2+(b_1+b_2)s+k_2]\,[m_2s^2+(b_2+b_s)s+(k_2+k_s)]\,[m_ws^2+(b_s+b_w)s+(k_s+k_w)]$$
$$- [m_ws^2+(b_s+b_w)s+(k_s+k_w)][b_2s+k_2]^2 - [m_1s^2+(b_1+b_2)s+k_2][b_ss+k_s]^2$$

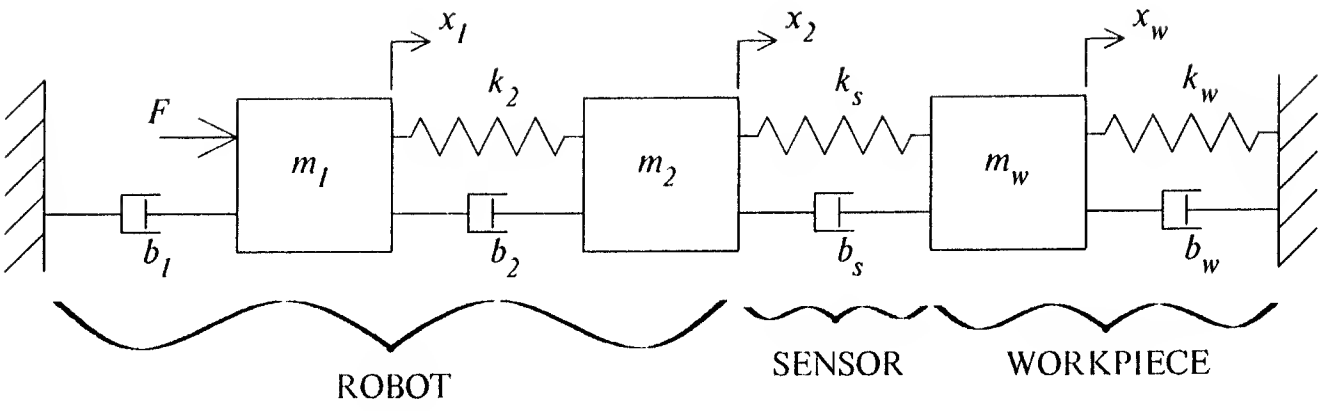

Figure 7: Robot system model including robot first mode and workpiece dynamics.

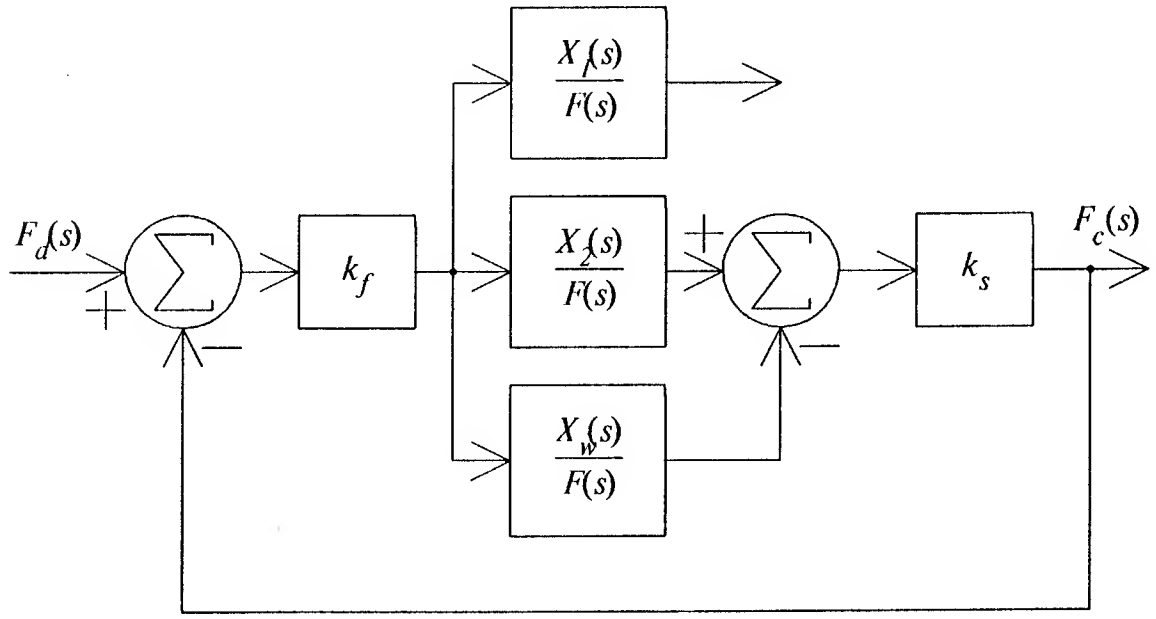

Figure 8: Block diagram for the controller of Figure 7.

The contact force is again the force across k_s

$$F_c = k_s(x_2 - x_w)$$

and the simple force control law is

$$F = k_f(F_d - F_c) \qquad (k_f \geq 0)$$

The block diagram for this controller, Figure 8, shows again that the feedforward path takes the difference between two open-loop transfer functions. This time, however, both of these transfer functions represent positions remote from the actuator force.

The root locus plot, Figure 9, shows a very interesting effect. The system is only

conditionally stable. For low values of k_f, the system is stable; for high values of k_f, the system is unstable; and for some critical value of the force feedback gain, the system is only marginally stable. The $\pm 60^{\circ}$ asymptotes result from the system's having six open-loop poles, but only three open-loop zeros. Inspection of the open-loop transfer functions confirms this: the numerator of the transfer function relating $X_2(s)$ to $F(s)$ is a third-order polynomial in s.

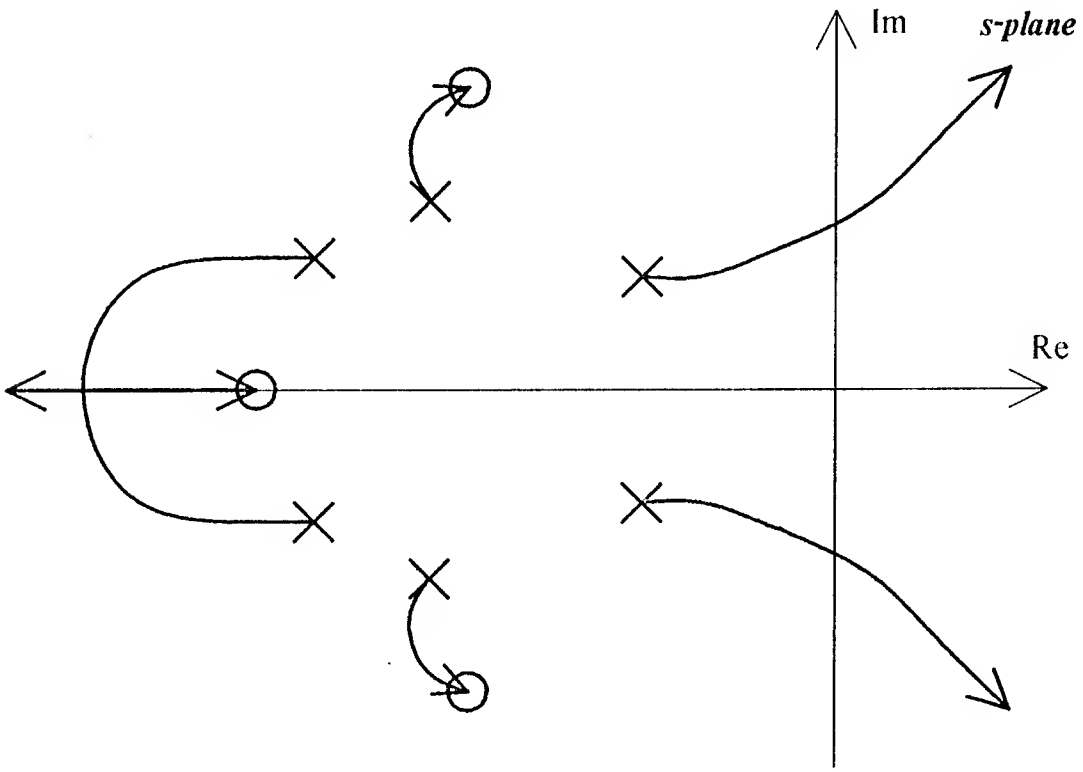

Figure 9: Root locus plot shape for the controller of Figure 7.

To provide some physical interpretation to this effect, note again that the input force F is applied to m_1, which moves with x_1. The sensor is attached to the robot at m_2, which moves with x_2. Here the controller attempts to regulate the contact force *through* the m_2-b_2-k_2 dynamic system. In the previous two examples, stability was achieved while the controller regulated the contact force on the single robot mass.

Exclude Workpiece Dynamics

To determine the influence of the workpiece dynamic characteristics on this system, their effects are now removed from the model. Figure 10 shows the workpiece modeled rigidly as a "wall". The robot model still includes both the rigid-body and first vibration modes. The sensor consists of a spring and damper between the robot and the workpiece.

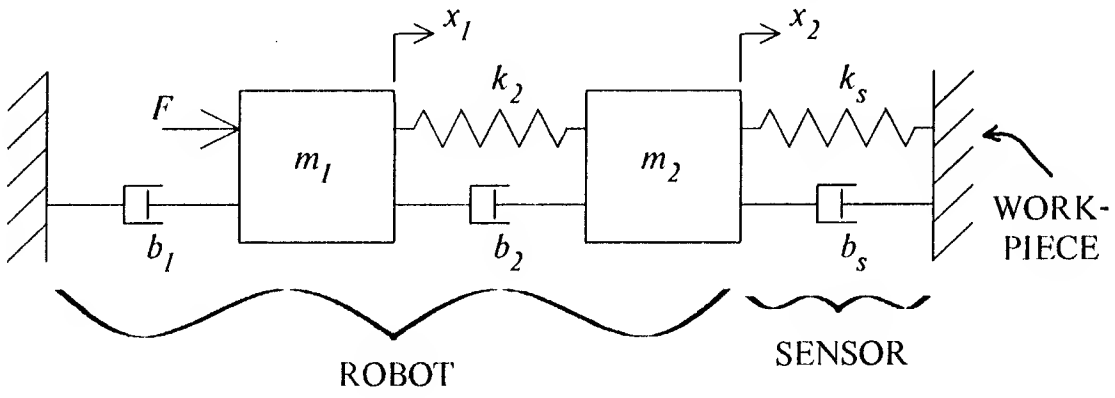

Figure 10: Robot system model including robot first mode and rigid workpiece.

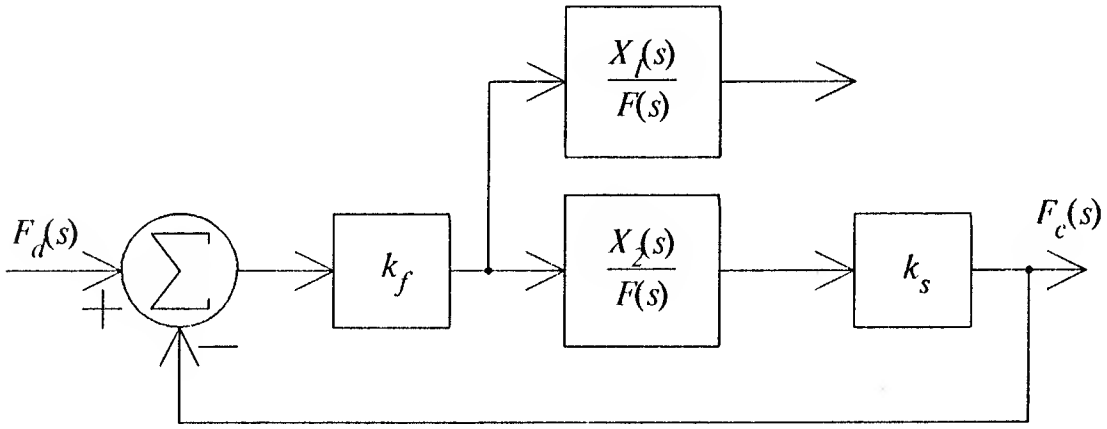

Figure 11: Block diagram for the controller of Figure 10.

This simpler two-mass model has only two state variables, x_1 and x_2, which measure the displacements of the two robot masses. The two open-loop transfer functions are:

$$\frac{X_1(s)}{F(s)} = \frac{m_2 s^2 + (b_s + b_2)s + (k_s + k_2)}{\text{<new 4}^{\text{th}}\text{-order characteristic polynomial>}}$$

$$\frac{X_2(s)}{F(s)} = \frac{b_2 s + k_2}{\text{<new 4}^{\text{th}}\text{-order characteristic polynomial>}}$$

where

<new 4th-order characteristic polynomial> =

$$[m_1 s^2+(b_1+b_2)s+k_2]\,[m_2 s^2+(b_2+b_s)s+(k_2+k_s)] - [b_2 s+k_2]^2$$

The contact force is given by

$$F_c = k_s x_2$$

and the control law will again be

$$F = k_f(F_d - F_c) \qquad (k_f \geq 0)$$

The block diagram for this controller, Figure 11, shows that no differences in open-loop transfer functions are being taken.

The root locus plot shape is shown in Figure 12. Again, the system is conditionally stable, as this time there is one open-loop zero and four poles. The instability is therefore shown to be present regardless of the workpiece dynamics (which may have been suspect in the above case of the model in Figure 7).

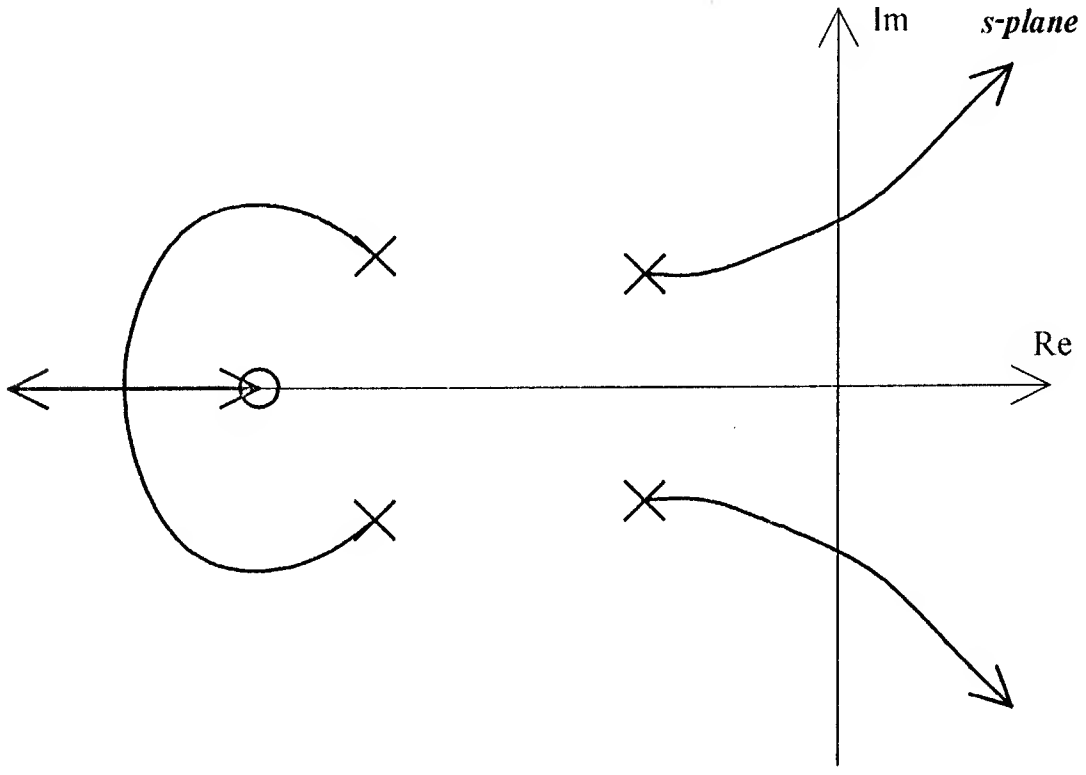

Figure 12: Root locus plot shape for the controller of Figure 10.

Comparison of the two-mass model of Figure 4 with that of Figure 10 shows that the models are basically the same (note the different subscripts), and the equations are therefore of the same form. One controlled system is stable (Figure 6), however, while the

other is not (Figure 12). The difference is only in the placement of the sensor. In the former, the feedback comes from the spring between the masses. In the latter, the feedback signal comes from the spring at the second mass to ground.

Conclusion

A series of lumped-parameter models has been developed in order to understand the effects of robot and workpiece dynamics on the stability of simple force-controlled systems.

An instability has been shown to exist for robot models which include representation of a first resonant mode for the arm. The mode modeled can be attributed to either drive-train or structural compliance (or both). The potential for instability is present because the sensor is then located at a point remote from the actuator. The controller attempts to regulate contact force through a dynamic system. (Compare the systems of Figures 7 and 10 with those of Figures 1 and 4.)

It must be noted, however, that there are many causes of force-controlled instabilities. The effect presented in this paper, that of robot structural dynamics, is an important problem in some systems. If the desired closed-loop bandwidth is low compared to the first mode frequency of the arm, then the target performance may be achievable. However, if we require a machine capable of higher performance, we must also investigate other issues carefully. In particular, the workpiece dynamics, actuator limitations, and controller implementation must be considered.

The effect of the workpiece dynamics is as yet unclear. Observation of force-controlled robotic systems suggests that the workpiece, when coupled through the force sensor, can significantly change the dynamics. Certainly if the workpiece were very compliant and extremely light, there could be no force across the sensor, degenerating the closed-loop system to the open-loop case, which of course is stable. In this paper we have demonstrated the opposite extreme, that when the workpiece is modeled as a rigid wall, the system can be unstable. The sensor and workpiece (environment) dynamics are therefore important and should be modeled. Limited actuator bandwidth, filtering, and digital controller implementation can also cause instability. These performance limitations must also be included in the system model that is used for controller design.

We have not addressed in this paper the effects of the discontinuity at the workpiece contact, the associated impact forces which occur, axis friction, or joint backlash. Nonlinear simulations suggest, however, that these effects can, under some conditions, lead to limit cycles in the otherwise stable linear systems, but they cannot stabilize the unstable linear systems. The stability bounds derived using the linear models should be used to set upper limits on the controller gains, which should then be decreased if limit cycles are observed under operating conditions.

The modeling and analysis techniques presented are tools to aid in control system design. For their accurate use, however, the models must sufficiently describe the actual hardware. A topic of on-going research is the comparison of these model predictions with experimental results. In particular, it is not clear how all the model parameters should be chosen in order to assure agreement between the analytical model and the experimental hardware.

References

[1] Cannon, R.H. and Schmitz, E.
Initial Experiments on the End-Point Control of a Flexible One-Link Robot.
The International Journal of Robotics Research, Fall 1984, Vol. 3, No. 3, pp 62-75.

[2] Eppinger, S.D., and Seering, W.P.
On Dynamic Models of Robot Force Control.
In *Proceedings of International Conference on Robotics and Automation.* IEEE, April 1986.

[3] Gevarter, W.B.
Basic Relations for Control of Flexible Vehicles.
AIAA Journal, April 1970, Vol. 8, No. 4, pp 666-672.

[4] Luh, Y.H.S., Fisher, W.D., and Paul, R.P.C.
Joint Torque Control by a Direct Feedback for Industrial Robots.
IEEE Transactions on Automatic Control, February 1983, Vol. AC-28, No. 2.

[5] Mason, M.T.
Compliance and Force Control For Computer Controlled Manipulators.
In *Transactions on Systems, Man, and Cybernetics.* IEEE, June 1981, Vol. SMC-11, No. 6, pp 418-432.

[6] Raibert, M.H. and Craig, J.J.
Hybrid Position/Force Control of Manipulators.
In *Journal of Dynamic Systems, Measurement and Control.* ASME, June 1981, Vol. 103, No. 2.

[7] Roberts, R.K., Paul, R.P., and Hillberry, B.M.
The Effect of Wrist Force Sensor Stiffness on the Control of Robot Manipulators.
In *Proceedings of International Conferenee on Robotics and Automation.* IEEE, March 1985.

[8] Salisbury, J.K.
Active Stiffness Control of a Manipulator in Cartesian Coordinates.
In *Proceedings of 19th Conference on Decision and Control*. IEEE, Vol. 1, December 1980.

[9] Whitney, D.E.
Historical Perspective and State of the Art in Robot Force Control.
In *Proceedings of International Conference on Robotics and Automation*. IEEE, March 1985.

This blank page was inserted to preserve pagination.

CS-TR Scanning Project
Document Control Form

Date : 10/26/95

Report # AIM-910

Each of the following should be identified by a checkmark:
Originating Department:

☒ Artificial Intellegence Laboratory (AI)
☐ Laboratory for Computer Science (LCS)

Document Type:

☐ Technical Report (TR) ☒ Technical Memo (TM)
☐ Other:_____

Document Information

Number of pages: 15 (19-IMAGES)
Not to include DOD forms, printer intstructions, etc... original pages only.

Originals are:
☒ Single-sided or
☐ Double-sided

Intended to be printed as :
☐ Single-sided or
☒ Double-sided

Print type:
☐ Typewriter ☐ Offset Press ☒ Laser Print
☐ InkJet Printer ☐ Unknown ☐ Other:_____

Check each if included with document:

☐ DOD Form ☐ Funding Agent Form ☐ Cover Page
☐ Spine ☐ Printers Notes ☐ Photo negatives
☐ Other: _____

Page Data:

Blank Pages(by page number):_____

Photographs/Tonal Material (by page number):_____

Other (note description/page number):

Description : Page Number:
IMAGE MAP: (1-15) UNIFIED TITLE PAGE 2-15
(16-19) SCANCONTROL, TRGT'S (3)

Scanning Agent Signoff:
Date Received: 10/26/95 Date Scanned: 11/6/95 Date Returned: 11/9/95

Scanning Agent Signature: Michael W. Cook

Scanning Agent Identification Target

Scanning of this document was supported in part by the **Corporation for National Research Initiatives,** using funds from the **Advanced Research Projects Agency** of the **United states Government** under Grant: **MDA972-92-J1029.**

The scanning agent for this project was the **Document Services** department of the **M.I.T Libraries.** Technical support for this project was also provided by the **M.I.T. Laboratory for Computer Sciences.**